vol. 48, n.° 1, enero-abril de 2026
ISSN impreso: 0120-0283 • ISSN en línea: 2145-8553

The discrepancy principle as an optimization method for a Gauss–Newton inversion scheme

Brayan Quiceno-Arenas[1]; Andrés Mauricio Muñoz-García[1]; Luis Duque-Gómez[*1]; Juan Paniagua-Castrillón[1]; Juan Navarro-Restrepo[1]; Moisés Bustamante-Rúa[2]

[1]Instituto Tecnológico Metropolitano, Medellín, Colombia. brayanquiceno250856@correo.itm.edu.co; andresmunoz@itm.edu.co; (*) luisduque@itm.edu.co; juanpaniagua@itm.edu.co; juannavarro@itm.edu.co
[2]Instituto de Minerales CIMEX, Universidad Nacional de Colombia, Medellín, Colombia. mobustan@unal.edu.co

Abstract

Geophysical inversion is a mathematical process used to infer subsurface features based on models that represent its physical properties according to measured data or physical parameters. One of the challenges in geophysical inversion is generating models that fit the data obtained. To address this, various methodologies, such as the Gauss-Newton scheme, have been developed. These methodologies require the optimal selection of the regularization parameter, yet they do not provide a predefined function or class for such selection. Consequently, this study proposes a novel optimization algorithm based on the discrepancy principle for estimating the regularization parameter using a set of synthetic and real electrical resistivity tomography data. According to the results, ideal tolerance values were obtained for each dataset, and the effectiveness and computational advantages of the proposed algorithm were demonstrated. Furthermore, the proposed algorithm displayed a better definition of the structures of interest than other algorithms reported in the scientific literature.

Keywords: Electrical resistivity tomography; Inversion; Gauss-Newton; Optimization.

El principio de discrepancia como método de optimización para un esquema de inversión de Gauss-Newton

Resumen

La inversión geofísica es un proceso matemático utilizado para inferir características del subsuelo a partir de modelos que representan sus propiedades físicas, según datos medidos o parámetros físicos. Uno de los retos de la inversión geofísica es generar modelos que se ajusten a los datos obtenidos. Para resolverlo, se han desarrollado diversas metodologías, como el esquema de Gauss-Newton. Estas metodologías requieren la selección óptima del parámetro de regularización, pero no proporcionan una función o clase predefinida para dicha selección. En consecuencia, este estudio propone un novedoso algoritmo de optimización, basado en el principio de discrepancia, para estimar

How to cite: Quiceno-Arenas, B.; Muñoz-García, A.M.; Duque-Gómez, L.; Paniagua-Castrillón, J.; Navarro-Restrepo, J.; Bustamante-Rúa, M. (2026). The discrepancy principle as an optimization method for a Gauss–Newton inversion scheme. *Boletín de Geología, 48*(1), 95-110. https://doi.org/10.18273/revbol.v48n1-2026006

el parámetro de regularización utilizando un conjunto de datos sintéticos y reales de tomografía de resistividad eléctrica. De acuerdo con los resultados, se obtuvieron valores ideales de tolerancia para cada conjunto de datos, y se demostró la eficacia y las ventajas computacionales del algoritmo propuesto. Además, el algoritmo mostró una mejor definición de las estructuras de interés que otros algoritmos reportados en la literatura científica.

Palabras clave: Tomografía de resistividad eléctrica; Inversión; Método Gauss-Newton; Optimización.

Introduction

For decades, the inversion problem has been a topic of great interest and impact in the field of computational geophysics. This makes it possible to infer the characteristics of a particular area by partially reconstructing the distribution of physical parameters obtained through geophysical exploration techniques (Tarantola, 2005; Isaev *et al*., 2022). Some of these parameters enable the inference of subsurface properties, including geological structure, magnetization, density, electrical resistivity, and electrical charge capacity (Reynolds, 2011; Sirota and Ivanov, 2018).

Resistivity is a measurement widely used in fields such as geotechnics, mining prospecting, hydrogeology, agriculture, and environmental sciences to gather and analyze information on subsoil's electrical properties related to composition, moisture content, salinity, and cohesion. Due to its applicability, methods have been developed in recent years for inverting data obtained by Electrical Resistivity Tomography (ERT). ERT is a non-destructive subsurface imaging technique that enables the detection of underground structures, water sources, and mineral deposits, as well as the conduct of geotechnical and environmental studies (Sjöberg *et al*., 2015; Berezowski *et al*., 2024). Resistivity data can be obtained at various resolutions and depths, depending on the electrode array, configuration, or matrix and the acquisition protocol used (Szalai and Szarka, 2008).

Some of the inversion methods used for ERT have been integrated into commercial software employing different approaches. For example, EarthImager™ 2D (Dastanboo *et al.*, 2020; Alpaslan, 2021; Capa-Camacho *et al.*, 2022; Zamanian *et al.*, 2023) employs inversion algorithms such as penalized least squares, smooth modeling, and robust inversion based on the Gauss-Newton and quasi-Newton methods on either a block or triangular mesh (Redhaounia *et al.*, 2015; Opatola *et al.*, 2022; Advanced Geosciences, Inc., 2023).

Similarly, Res2Dinv (Arjwech *et al.*, 2020; Aliou *et al.*, 2022; Chibani *et al.*, 2023) uses the fast least squares, damped least squares, and smooth-constrained least squares inversion algorithms modified based on the quasi-Newton, Marquardt-Occam (Marquardt method with constrained smoothness), and Gauss-Newton methods on either a block or unstructured mesh (Loke and Barker, 1996; Hellman *et al.*, 2016; Loke *et al.*, 2018; Zeynolabedin *et al.*, 2021; Oliveira *et al.*, 2023). AarhusInv (Mudler *et al.*, 2019; Andersen *et al.*, 2020; Genedi *et al.*, 2021; Finn *et al.*, 2022) utilizes the Laterally Constrained Inversion (LCI) and Spatially Constrained Inversion (SCI) algorithms based on the Gauss-Newton method with a Marquardt modification on either a block or triangular mesh (Auken and Christiansen, 2004; Auken *et al.*, 2015; Lin *et al.*, 2019).

Finally, ZondRes2D (Idfi *et al.*, 2019; Kukemilks and Wagner, 2021) features the regularized least squares inversion algorithm based on the Gauss-Newton, incomplete Gauss-Newton, and nonlinear conjugate gradient methods on a block mesh (Zond Software, 2022). Additionally, to calculate resistivity values, these tools typically employ the finite difference method for data collected in regions with flat layers, and finite elements for data collected in regions with more complex topographies (Loke *et al.*, 2018). Moreover, these inversion methods are used in some open-source environments based on C++ and Python, including BERT, pyGIMLi, pyres, ResIPy, and SimPEG (Doyoro *et al.*, 2022). These packages emerge as an alternative solution to some of the drawbacks found in commercial software, such as the inability to filter out current and potential electrode noise, remove outliers, and modify resistivity maps by manipulating ERT data. Such drawbacks require the use of additional computational tools (*e.g.*, x2ipi and Prosys), self-created routines, among other strategies (Placencia-Gómez *et al.*, 2010; Bingham and Legault, 2018; Azaiez *et al.*, 2020; Porras *et al.*, 2022; Yonli *et al.*, 2023).

Regarding inversion results, while Res2Dinv is fast and efficient, it struggles to adapt to non-rectangular topographies, resulting in vertical expansion in the generated data. Conversely, while AarhusInv is algorithmically more complex and slower than Res2Dinv, it adapts better to complex topographies. However, it also tends to produce horizontal

expansions. PyGIMLi falls somewhere between Res2Dinv and AarhusInv in terms of speed and adaptability. Nonetheless, it is not effective in solving structures with sharp geometries, leading to rounded anomalies. This problem can be minimized by properly adjusting the regularization parameter λ in the pre-weighted Gauss-Newton scheme, which is iteratively employed with ridge regularization (Tikhonov regularization) (Hellman *et al.*, 2016; Rücker *et al.*, 2017; Von Bülow *et al.*, 2021; Jabrane *et al.*, 2023). One of the challenges in employing Tikhonov regularization in models or schemes like pyGIMLi is finding the most efficient approach for solving this inverse problem considering that the parameters obtained from geophysical exploration are non-linear. The regularization parameter λ, which controls the balance between data fidelity and prior information, allows us to reach the solution to the inverse problem that is more suited to its characteristics and correct the rounded anomalies found in the framework (Oraintara *et al.*, 2000). Different methods have been developed to estimate this parameter, including maximum likelihood (ML), ordinary cross-validation (OCV), generalized cross-validation (GCV), the discrepancy principle (DP) (Morozov, 1984; Okamoto and Li, 2007), the L-curve (Quiceno *et al.*, 2022), and genetic algorithms (GA) (Wu *et al.*, 2008; Zheng *et al.*, 2019). Since pyGIMLi lacks a function or class to estimate the optimal λ value, it is common practice to use trial-and-error methodologies to find it. For example, Quiceno *et al.* (2022) developed an algorithm based on the L-curve in conjunction with a curvature function to semi-automatically estimate it.

The discrepancy principle (DP) selects the regularization parameter by enforcing that the residual norm of the reconstructed solution remains commensurate with the estimated noise or error level in the data. In essence, it constrains the solution to remain within the fidelity limits imposed by the data quality, thus mitigating overfitting and underfitting. Originally formulated by Morozov (1984), building upon foundational work dating back to the 1960s, the DP has become a well-established and rigorous criterion within the broader framework of Tikhonov regularization for addressing ill-posed inverse problems in which noise may strongly influence the solution.

In contrast to the DP, methods such as maximum likelihood (ML), cross-validation (CV), and generalized cross-validation (GCV) rely explicitly on statistical assumptions regarding noise characteristics and data structure. Other strategies, such as the L-curve method or genetic algorithms (GA), tend to introduce a higher degree of subjective interpretation, particularly under conditions of severe noise or strong ill-posedness, as is commonly encountered in electrical resistivity tomography (ERT). In such contexts, the DP offers an intuitive and model-agnostic criterion whose reduced dependence on specific probabilistic assumptions facilitates its practical adoption and enhances confidence in the stability of the resulting solutions.

This paper describes the implementation and validation of a consecutive approximation algorithm based on the discrepancy principle to automatically estimate the optimal λ value in the pre-weighted Gauss-Newton inversion scheme.

The algorithm was validated using three datasets from different sources and characteristics to thoroughly test its effectiveness in various contexts and applications. The first dataset is a synthetic mixed anomaly model in homogeneous layers taken from an example in the pyGIMLi library. The second dataset corresponds to a replicated synthetic model of conductive blocks. Lastly, the third dataset is a slag dump profile, which is also available as an example in the same library but was originally described and employed in 2006.

Materials and methods

Gauss-Newton scheme and discrepancy principle

Tikhonov regularization is a widely used method for solving ill-conditioned problems by introducing a regularization term that modifies the objective function of a system (Sirota and Ivanov, 2018). Equation 1 shows a general expression that describes the operation of Tikhonov regularization, where Φ_d is generally a measure of the error between the model predictions and the actual data, known as the residual norm. For its part, Φ_m is a regularization term that imposes constraints such as L1 or L2, where a sum of absolute values or the square root of the sum of squares is applied to the possible values of Φ_m, so it is known as the solution norm (Tikhonov, 1963, 1966; Willoughby, 1979; Tikhonov *et al.*, 1995).

$$\min_{x_\lambda \in \mathbb{R}^n} \{\Phi = \Phi_d + \lambda \Phi_m\}. \quad (1)$$

The regularization parameter λ is the value that controls the balance between data fidelity and prior information. In other words, it maintains the balance between the Φ_d and Φ_m norms, and hence the result of the objective

function that requires to be minimized. This concept is crucial in the pre-weighted Gauss-Newton scheme used in pyGIMLi and shown in equation (2):

$$\underset{x_\lambda \in \mathbb{R}^n}{min}\{\psi = \|D(d - f(m))\|_2^2 + \lambda\|C(m - m^0)\|_2^2\}, \quad (2)$$

where $\|D(d - f(m))\|_2^2$ is the residual norm and $\|C(m - m^0)\|_2^2$ is the solution norm. Here, D is the diagonal matrix of the relative error; d is the logarithmic apparent resistivity vector; m is the logarithmic resistance vector; $f(m)$ is the response model of m; and C corresponds to the identity if m^0 is a model with a priori information, or serves as a feature control of the scheme if m^0 is a constant vector (Rücker, 2011; Quiceno-Arenas *et al.*, 2022).

The discrepancy principle will be used to select λ. According to this principle, λ can be chosen when the following equality is achieved:

$$\|D(d - f(m))\|_2^2 = \eta\varepsilon, \quad (3)$$

where η is the tolerance value (preferably ≥1) and ε is the error size (Sizikov and Sidorov, 2017; Schenkels and Vanroose, 2018). In the case of Gauss-Newton methods, where the dataset covariance is known, as in the pyGIMLi inversion scheme, the error size is proportional to the N data size (Günther, 2004; Petra *et al.*, 2012). Therefore, a value $\eta = 1$ is expected to lead to a residual norm equal to the data size:

$$\|D(d - f(m))\|_2^2 = N. \quad (4)$$

Thus, the optimal λ value is obtained by satisfying equation (4).

Datasets

Mixed anomaly model in homogeneous layers: This dataset corresponds to a synthetic model that features mixed anomalies and is characterized by a flat topography with three homogeneous layers, each with defined apparent resistivity data. The second layer includes a uniform and a non-uniform structure as anomalies, which also have a defined apparent resistivity value (Figure 1) (pyGIMLi, 2023a). Resistivity data were collected using a Dipole-Dipole electrode array with a spacing of 1.5 meters, a Gaussian noise of 1%, and a voltage error of approximately 1 μV.

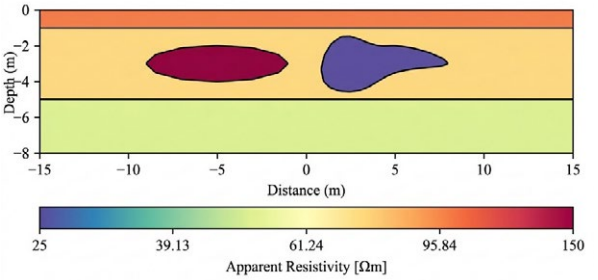
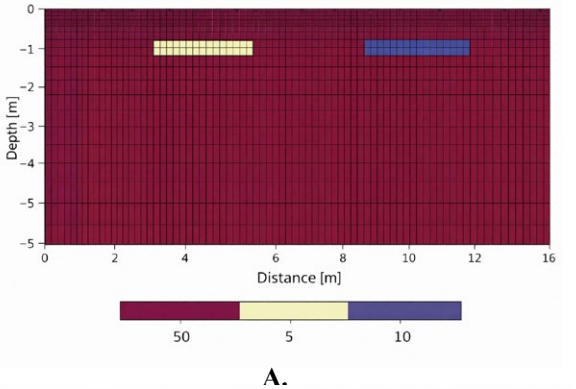
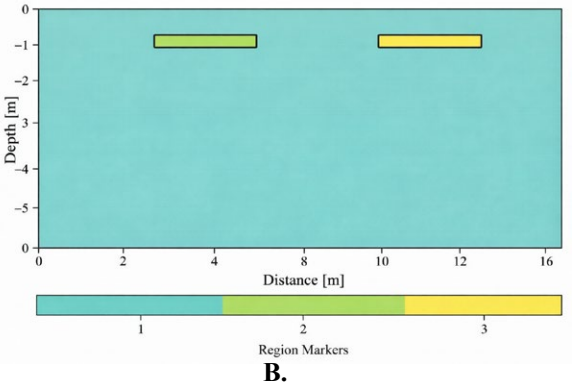


Figure 1. Mixed anomaly model in homogeneous layers (pyGIMLi, 2023a).

Conductive block model: This model features a length of 16.2 meters and a depth of 5.4 meters. It has a flat topography and contains two conductive blocks of 2.5 meters in length and 0.3 meters in height (Figure 2) (Zamanian *et al.*, 2023). The ResIP framework was used to perform the modeling, employing Dipole-Dipole, Wenner α, Schlumberger, and Multi-gradient electrode arrays with a spacing of 0.6 meters and a Gaussian noise of 2%. Figure 2A shows the synthetic model created in pyGIMLi, where Region 1 (50 Ωm) represents the background layer and Region 2 (5 Ωm) and Region 3 (10 Ωm), the conductive blocks.



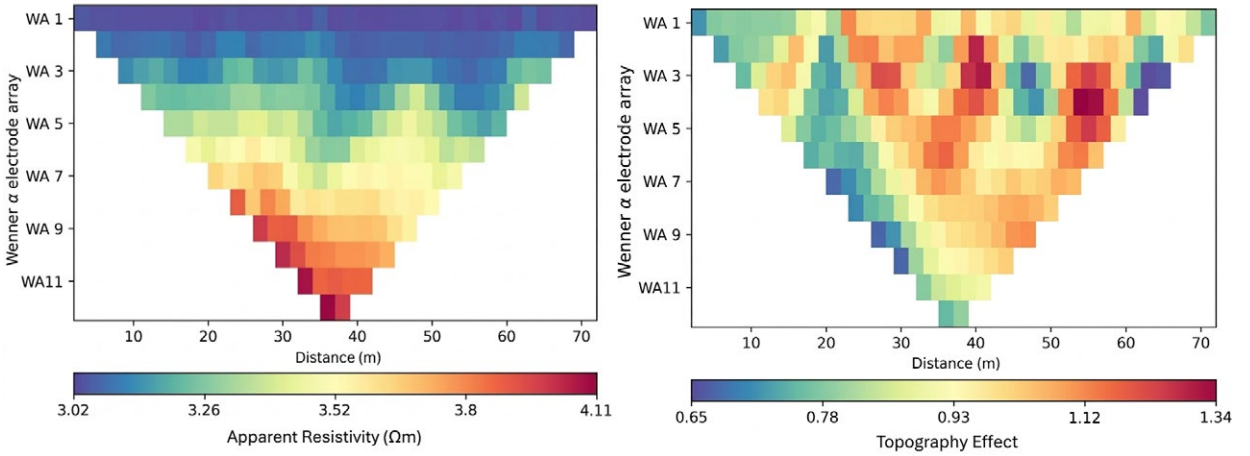
A.



B.

Figure 2. Synthetic conductive block model. **A.** Adapted from Zamanian *et al.* (2023) and **B.** created in pyGIMLi.

Real slag dump data: This dataset corresponds to a slag dump from steel production, which features a width of 70 meters and a maximum height of 14 meters above ground level. A total of 222 data points were collected using a Wenner α electrode array with a spacing of 2 meters (Günther *et al.*, 2006). At its electrodes, the minimum and maximum elevation recorded was 108.45 meters and 121.20 meters, respectively (pyGIMLi, 2023b). Figure 3 displays the distribution of the samples taken using pseudosections from the electrode array and spacing along with the apparent resistivity values (Figure 3A) and topographic effect values for such data (Figure 3B). The topographic effect values were obtained by computing the ratio between the numerically calculated geometric factor that accounts for topography and the analytical formula that does not.



A. **B.**

Figure 3. Pseudosections from electrode array and spacing of the **A.** apparent resistivity values and **B.** topographic effect (pyGIMLi, 2023b). WA refers to Wenner α, and the value next to it to the electrode spacing applied in the data acquisition protocol.

Consecutive approximation algorithm and inversion parameters

The pseudocode shown in Algorithm 1 describes the process for estimating the optimal λ value for arbitrary datasets that depend on solving the inverse problem. Given that the ERT inversion manager in pyGIMLi allows the value of Φ_d to be estimated for an inversion with specific parameters, an iterative process must be carried out for the various ranges of λ that are evaluated. Also, another iterative process must be performed to evaluate each value of that range to arrive at the approximation that is most consistent with the ideal value. Since the algorithm makes it possible to assign an initial range for λ, as well as an initial number of samples and the number of epochs to be run, the proposed approach may adapt to the different datasets that can be processed. The inversion parameters (*i.e.*, the inversion characteristics of the scheme) included the maximum cell size of the unstructured mesh (paraMaxCellSize) and the boundary extrapolation (paraBoundary). Moreover, it is worth noting that η is the output parameter of X^2 in pyGIMLi.

Algorithm 1. Selection of the regularization parameter in pyGIMLi using consecutive approximation and the discrepancy principle.

Input: α (dataset), λ_{it} (initial λ of the range to evaluate in the first and subsequent epochs), λ_{fn} (final λ of the range to evaluate in the first and subsequent epochs),n_0 (number of samples in the first epoch), n (number of samples in the subsequent epochs) ω (width of the search range), E (number of epochs), and β (inversion parameters).

Output: λ_{cl} (regularization parameter where Φ_d is closest to or equal to N).

Constants: ω_o (width of the search range in the first epoch), and ω_h (half of ω).

Variables: Δ (absolute difference between N and Φ_d), and Λ (λ close to N).

Initialize:

$\psi \leftarrow$ object (ERT manager instantiated with α)

$\theta \leftarrow 0$ (adjustment of the search range)

$\Lambda_i \leftarrow \emptyset$ (set of λ close to N)

$\Delta_{min} \leftarrow \infty$ (minimum value of Δ)

Process:

$\omega_o \leftarrow \lambda_{fn} - \lambda_{it}$

$\omega_h \leftarrow \frac{\omega}{2}$

$N \leftarrow |\alpha|$

if $\omega_o < 1$ **then**

  $\theta \leftarrow 1$

for $t \leftarrow 0$ **to** $E - 1$ **do**

  if $t = 0$ **do**

    $\lambda_i \leftarrow \left\{\lambda_{it},\ \lambda_{it}+1\frac{\omega_o}{n-1},\ \lambda_{it}+2\frac{\omega_o}{n-1},\ \lambda_{it}+(n-2)\frac{\omega_o}{n-1},\ \lambda_{it}+\omega_o\right\}$

  else if $t > 0$ **do**

    $\lambda_i \leftarrow \left\{\lambda_{it},\ \lambda_{it}+1\frac{\omega}{n-1},\ \lambda_{it}+2\frac{\omega}{n-1},\ \lambda_{it}+(n-2)\frac{\omega}{n-1},\ \lambda_{it}+\omega\right\}$

  $\Delta \leftarrow \infty$

  for each λ **in** λ_i **do**

    perform inversion using ψ with β

    $\Phi_d \leftarrow \Phi_d \in \psi$

    if $|N - \Phi_d| < \Delta$ **do**

      $\Lambda \leftarrow \lambda$

      $\Delta \leftarrow |N - \Phi_d|$

      if $\Delta < \Delta_{min}$ **do**

        $\lambda_{cl} \leftarrow \Lambda$

        $\Delta_{min} \leftarrow \Delta$

  $\Lambda_i \leftarrow \Lambda_i \cup \{\Lambda\}$

  $\lambda_{it} \leftarrow \Lambda - \frac{\omega_h}{10^{t+\theta}}$

  $\lambda_{fn} \leftarrow \Lambda + \frac{\omega_h}{10^{t+\theta}}$

  if $t \geq 2$ **do**

    if $\Lambda_{t-1} = \Lambda_{t-2}$ **do**

      end

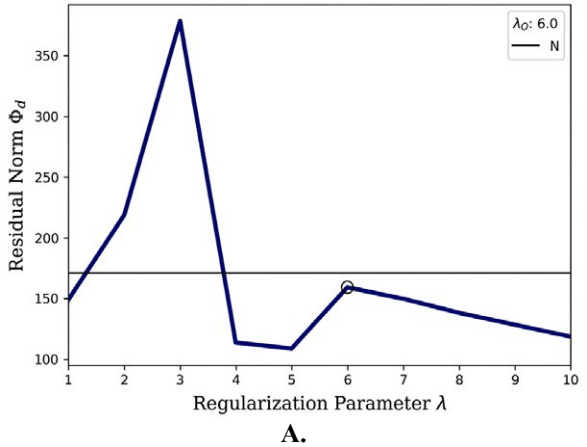
Note: The notation | | in a set refers to its cardinality.

Results and discussion

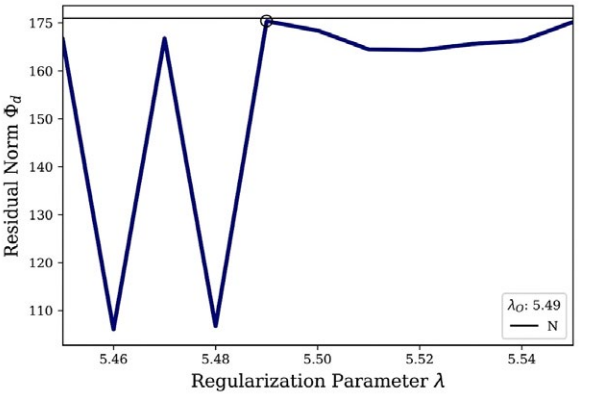
The results section provides a comprehensive validation of the consecutive approximation algorithm (Algorithm 1), which was designed to automatically determine the optimal regularization parameter (λ_0) within the pre-weighted Gauss-Newton inversion scheme. The primary objective of the validation was to demonstrate that the algorithm could robustly converge on a λ value that satisfies the discrepancy principle, resulting in an ideal tolerance value ($X^2 \approx 1.00$) across various data scenarios. This target X^2 value signifies that the error between the model and the data aligns perfectly with the data size, indicating a highly accurate and ideal fit.

The algorithm's performance was assessed using two synthetic Electrical Resistivity Tomography (ERT) models—one with a mixed anomaly in homogeneous layers and another with a conductive block—as well as a real-world slag dump profile. In all tests, the proposed method successfully converged to the optimal λ within a limited number of epochs, consistently yielding inversion models with X^2 values precisely at or near 1.00. Furthermore, a comparative analysis against an L-curve-based approach (Algorithm 2) revealed that the proposed Algorithm 1 offers superior automation, greater self-sufficiency, and enhanced computational efficiency. Crucially, the resulting inversion models, particularly those for the synthetic conductive block, demonstrated improved subsurface structure definition and better handling of background layer distribution, showcasing its practical advantage over other established inversion frameworks.

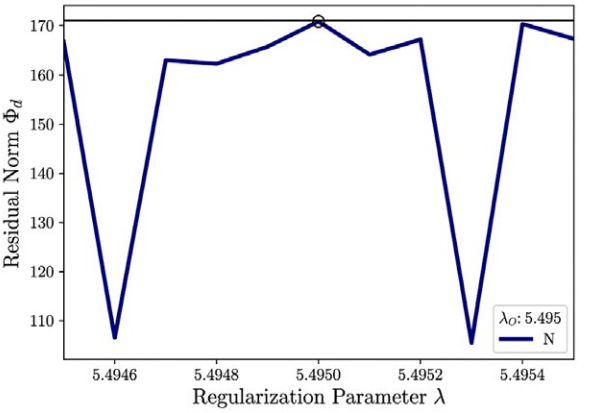
Figure 4 presents the approximation results for the estimation of λ in the synthetic mixed anomaly model in homogeneous layers using the proposed method. As shown in Figure 4C, the optimal value was found at epoch 5. Figure 5 shows the response model obtained with the optimal regularization parameter (λ_0), where the ideal tolerance value (X^2=1) was achieved.



A.



B.



C.

Figure 4. Discrepancy curve (D-curve) for epoch 1 **A.**, 3 **B.**, and 5 **C.** in the synthetic dataset.

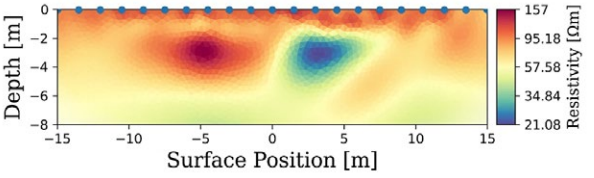


Figure 5. Unstructured mesh response model (ERT) in the synthetic mixed anomaly model in homogeneous layers with λ_0= 5.4746, using the consecutive approximation algorithm.

Figure 6 displays the optimized response model in the mixed anomaly model in homogeneous layers (Figure 1). It was obtained using an algorithm that combines the L-curve and a curvature function (see Algorithm 2) to estimate the optimal regularization parameter (Quiceno *et al.*, 2022).

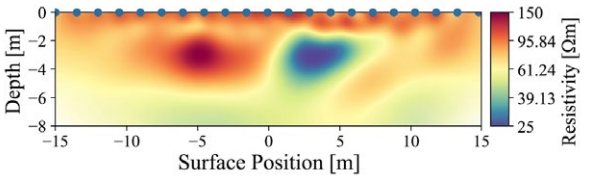


Figure 6. Unstructured mesh response model (ERT) in the synthetic mixed anomaly model in homogeneous layers with L-curve. From Quiceno *et al.* (2022).

Algorithm 2. Selection of the regularization parameter in pyGIMLi using the L-curve method.

Require: Range of λ values (λ_i ... λ_f).

Ensure: λ_o (optimal regularization parameter).

Process:

Create a function to numerical derivation
Call the ERT inversion manager

for $\lambda \leftarrow \lambda_i$ **until** λ_f **do**

Initialize inversion with λ
$\rho \leftarrow \Phi_d$
$\eta \leftarrow \Phi_m$

Define function γ
$\lambda_o \leftarrow$ Maximum value of γ

Note:
Adapted from Quiceno *et al.* (2022).

There is a high correlation between the data processed in both the response model obtained with the L-curve method and the response model obtained with the discrepancy principle. The anomalies introduced in the modeling process, along with a significant portion of the homogeneous layer distribution, can be differentiated. However, it is worth noting that the inversion parameters were not the same when the two proposed algorithms were validated.

When the results of Algorithm 2 (L-curve method) were compared with those of Algorithm 1 (consecutive approximation), the latter was found to be significantly more automated and self-sufficient because it can easily adapt to more flexible or critical search regions that change gradually with each epoch. This simplifies the learning curve and application of the proposed algorithm for the final user, making it considerably more useful and less laborious. Finally, by avoiding the repetitiveness of λ_O and successfully managing to automatically adapt to the number of samples n in the successive search regions, Algorithm 1 significantly outperformed Algorithm 2 in terms of the computational resource and time required to obtain the best regularization parameter.

In the case of the slag dump, Figure 7 shows the approximation results for the estimation of λ_O using the proposed method. The optimal value was achieved at epoch 5 (see Figure 7C). Furthermore, Figure 8 displays the response model obtained with the estimated λ_O value, where, as expected, an ideal tolerance value was achieved.

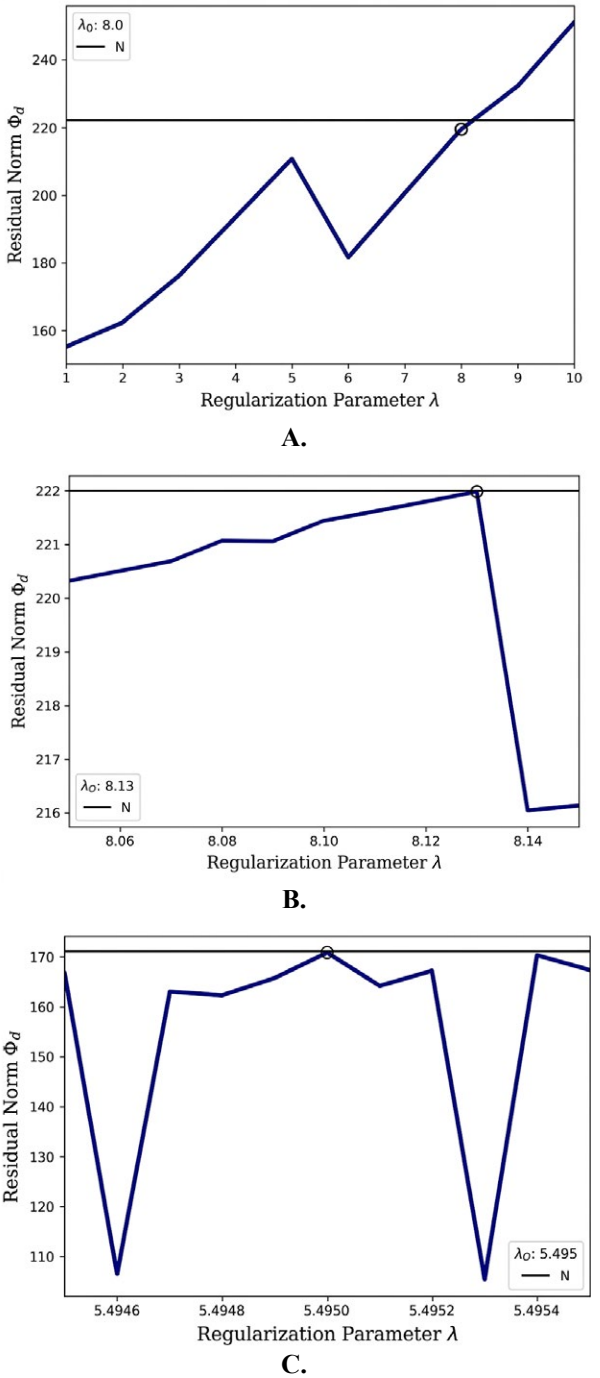


Figure 7. Discrepancy curve (D-curve) for epoch 1 **A.**, 3 **B.**, and 5 **C.** in the real slag dump dataset.

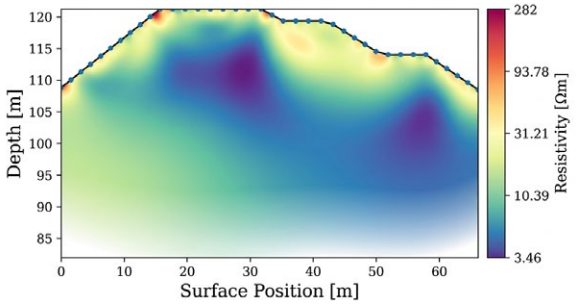


Figure 8. Unstructured mesh response model (ERT) in the real slag dump dataset with λ_O= 8.1315.

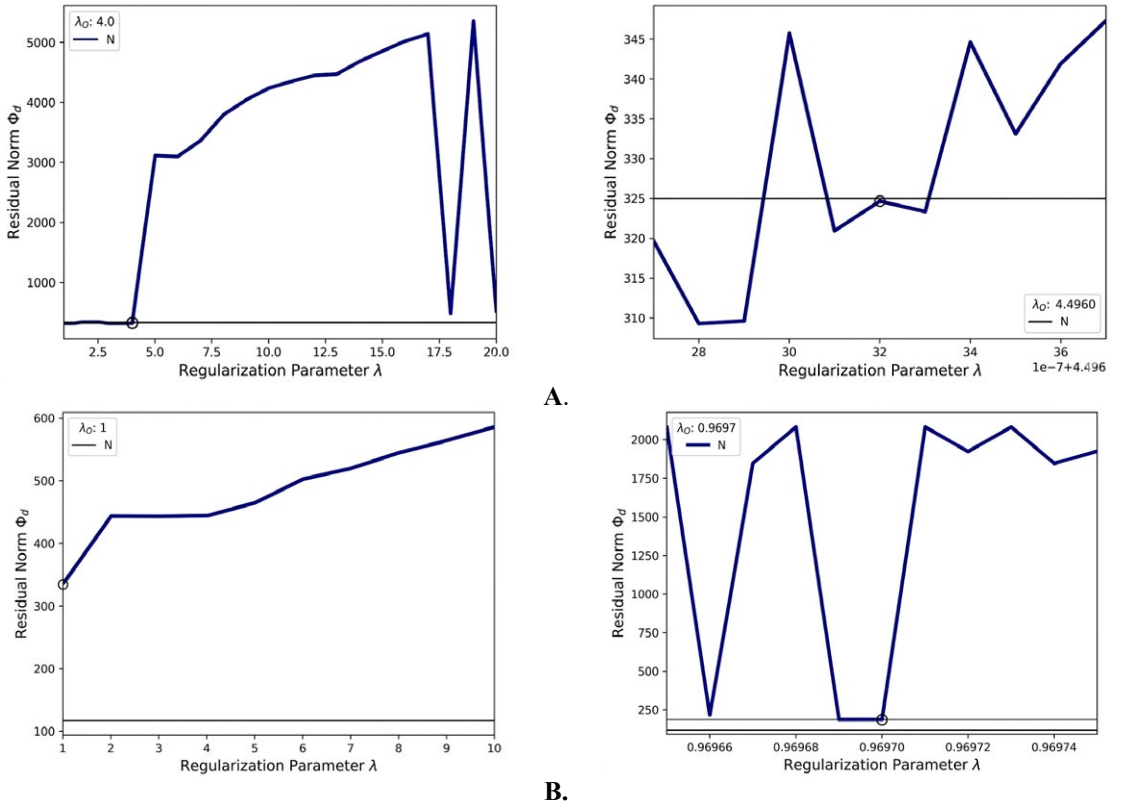
Table 1 contains the optimization process parameters used in the mixed anomaly model in homogeneous layers and the slag dump profile.

Table 1. Optimization and inversion process parameters of the mixed anomaly model in homogeneous layers and the slag dump profile.

Dataset	Algorithm				Inversion		Output			
	λ_i	λ_f	n	E	MaxCell	Boundary	λ_o	E_o [(b)]	χ^2	RRMS[(c)] (%)
MAMHL[(a)]	1	10	10	5	0.1	0	5.4746	5	1	1.00
Slag dump							8.1315			3.00

[(a)]MAMHL = mixed anomaly model in homogeneous layers. [(b)]RRMS = relative root mean square. [(c)]It represents the epoch where the optimal λ value was found.

Finally, Figure 9 shows the approximation results for the estimation of λ in the conductive block model. The D-curves for the first iteration are shown in the left column, and the D-curves for the optimal λ value are shown in the right column. Figures 9A, 9B, 9C and 9D correspond to the Dipole-Dipole, Wenner α, Schlumberger, and Multi-gradient electrode arrays.



A.

B.

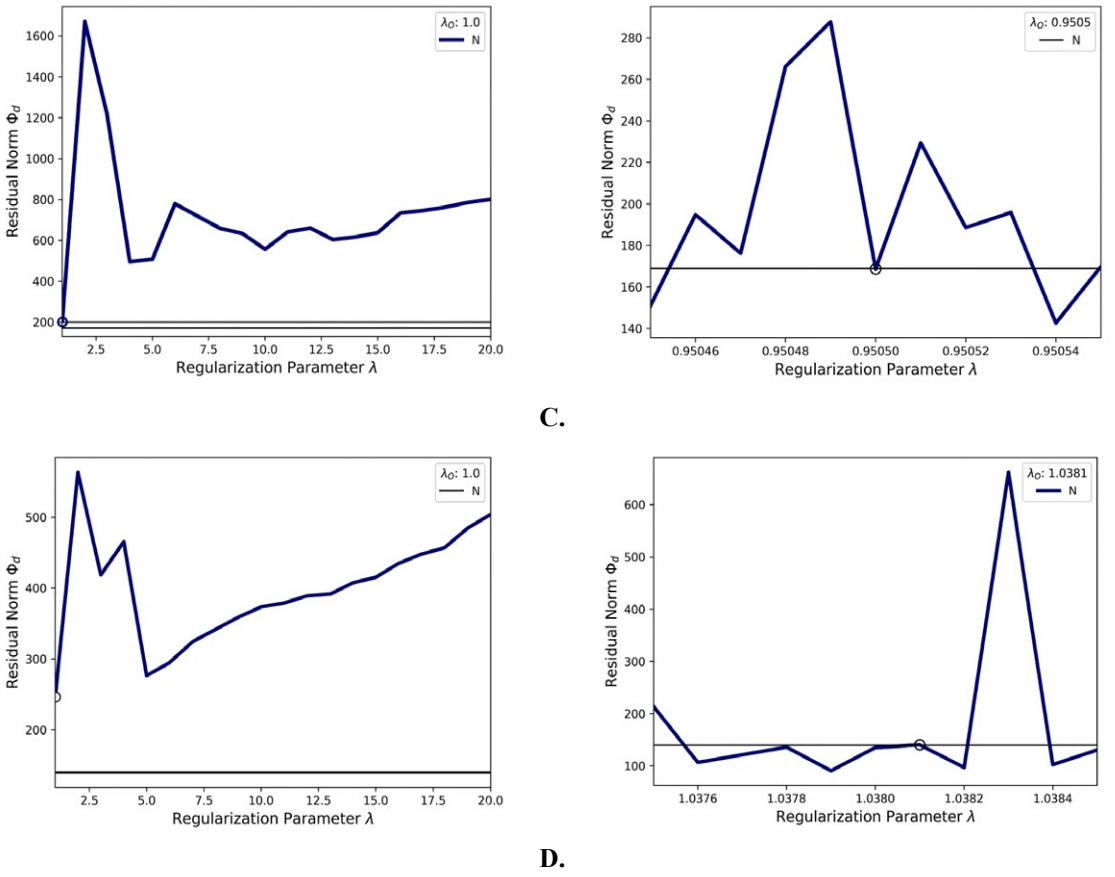


Figure 9. Discrepancy curves (D-curves) of the initial and final epochs for the optimal λ value in the four electrode arrays employed in the conductive block model. **A**. Dipole-Dipole, **B**. Wenner, **C**. Schlumberger and **D**. Multi-gradient.

Table 2 contains the technical information gathered from the conductive block modeling with the different electrode arrays. Each dataset showed an absolute relative error of 2%, which indicates clean Gaussian noise in the modeling process when using a voltage error of approximately 0.1 μV.

Table 2. Technical information of the conductive block model datasets.

Array	N[(a)]	Error[(b)]	
		Min (%)	Max (%)
Dipole-Dipole	325	2	2
Wenner α	117		
Schlumberger	169		
Multi-gradient	140		

[(a)]Amount of data obtained with the pyGIMLi modeling protocol for each array. [(b)]Relative error of the dataset.

Table 3 lists both the parameters used in Algorithm 1 and the parameters obtained from the inversion with the λ_O value found.

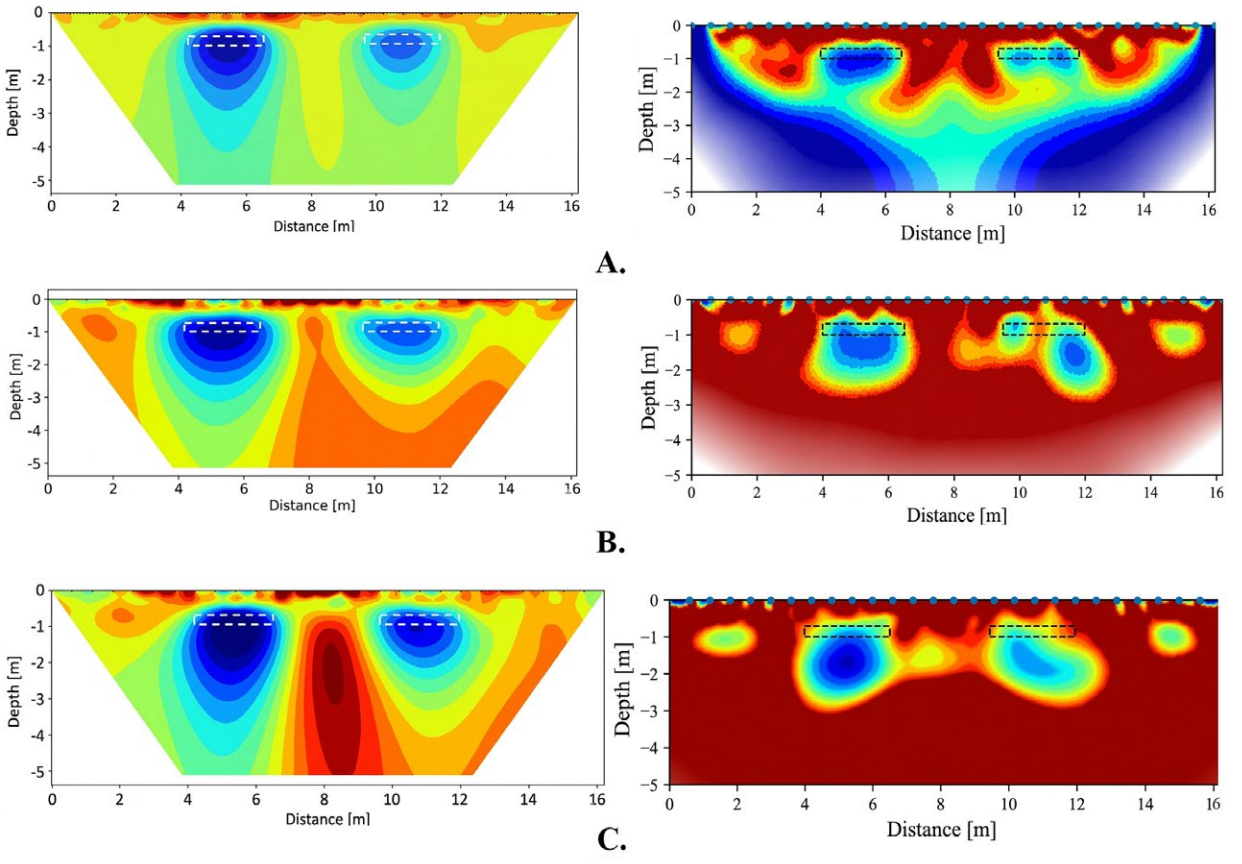
Table 3. Optimization and inversion process parameters of the conductive block model datasets.

Array	Algorithm				Inversion		Output			
	λ_i	λ_f	n	E	MaxCellSize	Boundary	λ_o	Eo[(a)]	χ^2	RRMS[(b)] (%)
Dipole-Dipole	1	20	20	10	0.005	0	4.496003	8	1	1.00
Wenner α							1.0381	6	2.24	2.90
Schlumberger							0.9505	6	0.99	1.98
Multi-gradient	1	10	10	10	0.01		1.0394	5	0.82	1.80

[(a)]RRMS = relative root mean square. [(b)]It represents the epoch where the optimal λ value was found.

After comparing the relative error of the dataset and the relative error obtained from the inversion with λ_o, and after analyzing the relative error obtained for the first two datasets (Table 1), we observe that the response model fits the absolute relative error (i.e., the error size ε) by obtaining an ideal tolerance value (or a value close to it). This indicates an ideal fit between the response model and the dataset, in contrast to obtaining a relative error better than the induced Gaussian noise, as is the case of Zamanian *et al.* (2023), with a RRMS lower than 1.2% in their response models.

In Figure 10, the response models obtained in ResIP (Zamanian *et al.*, 2023) are displayed in the left column and those optimized with pyGIMLi, in the right column. Figures 10A, 10B, 10C, and 10D correspond to the Dipole-Dipole, Wenner α, Schlumberger, and Multi-gradient electrode arrays, respectively.



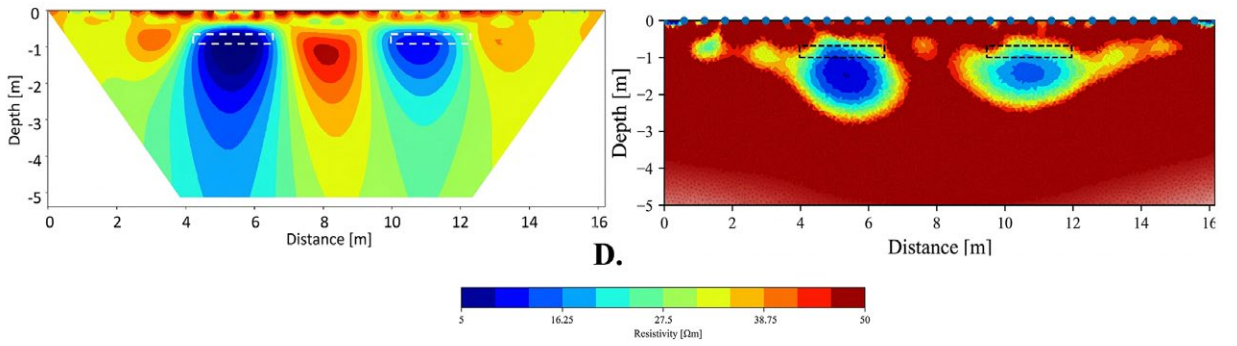


Figure 10. Response models (ERT) with ResIP and pyGIMLi (with λ_o) for the four electrode arrays employed in the conductive block model. **A.** Dipole-Dipole. **B.** Wenner α. **C.** Schlumberger. **D.** Multi-gradient.

When compared to each response model, the proposed algorithm demonstrates an improved distribution of the background layer and reduced vertical expansion of the conductive blocks. This improvement is attributed to better control of the rounded anomaly resulting from the optimal regularization parameter. However, a vertical displacement with respect to the original positions of the conductor blocks has been observed, which could be attributable to the configuration of each array. Particularly, the Dipole-Dipole array stands out for having good vertical resolution and considerable depth of investigation. Conversely, the Wenner α, Schlumberger, and Multi-gradient arrays, while displaying good horizontal and lateral resolution, do not achieve comparable depth of investigation (Szalai *et al.*, 2009; Loke *et al.*, 2018). Table 4 shows the comparison between the different arrangements.

Table 4. Comparison between the different arrangements.

Array	Dominant sensitivity	Depth of investigation	Inversion resolution
Dipolo–Dipolo	Lateral: High	High	High
Wenner-α	Vertical: High	Moderate	Low/Medium
Schlumberger	Mixed: Moderate	Medium/High	Medium
Multigradiente	Mixed: High	High	Very High

Regarding the obtained E_O, it is important to consider that the optimal regularization parameter may not always be achieved in the final epoch. This is because there may be even closer proximity to N in the initial or intermediate iterations, as seen in the conductive block model. Therefore, Algorithm 1 considers this selection criterion to deliver the optimal regularization parameter.

Furthermore, prior knowledge of the data (*e.g.*, number of samples) is crucial to define the initial search region (range of λ values) that best fits the difference between the theoretical and generated or observed values (Wang *et al.*, 2010). Nonetheless, choosing a search region smaller or larger than 1 does not affect the functionality of the consecutive approximation algorithm, as it has built-in compensation for the designated search region during implementation.

Conclusions

The consecutive approximation algorithm proposed in this study enabled us to estimate the optimal regularization parameter for solving the inverse problem using the Gauss-Newton scheme and ERT data.

The proposed algorithm was validated using both synthetic and real data and compared with another algorithm based on the L-curve method (see Algortithm 2) (Quiceno *et al.*, 2022). According to the results, the proposed algorithm was able to estimate an optimal value for the regularization parameter (λ), with good correlation between the observed and theoretical data, as well as an ideal tolerance (X^2) for both datasets.

Although the response models of the two algorithms (*i.e.*, the L-curve algorithm and the one proposed in this study) exhibit similarities in the obtained images, the proposed consecutive approximation algorithm proved to be more efficient and flexible. This is because the regularization parameter estimation no longer involves previously assigned search intervals or trial-and-error testing. These advantages make the proposed algorithm -based on the discrepancy principle- a promising tool for geophysical data inversion, as it can adapt to different datasets, numbers of measurements, and search regions, facilitating its use in a variety of scenarios. Considering this, the results of this study contribute to enhancing the processing and interpretation of ERT data and provide a foundation for future research on related methods or applications.

Acknowledgments

This study was funded by Minciencias through research project RC0756 of 2022. In addition, we would like to thank the staff of the Computer Science Laboratory at the Instituto Tecnológico Metropolitano for all the support provided, and ITM Translation Agency translated the manuscript into English.

References

Advanced Geosciences Inc. (2023). AGI EarthImager 2D. https://www.agiusa.com/agi-earthimager-2d

Aliou, A.S.; Dzikunoo, E.A.; Yidana, S.M.; Loh, Y.; Chegbeleh, L.P. (2022). Investigation of geophysical signatures for successful exploration of groundwater in highly indurated sedimentary basins: a look at the Nasia Basin, NE Ghana. *Natural Resources Research, 31*(6), 3223-3251. https://doi.org/10.1007/s11053-022-10125-9

Alpaslan, N. (2021). Determination of borehole locations and saline-water intrusion for groundwater in Central Anatolia Region, Turkey using electrical tomography (ERT) method. *Environmental Earth Sciences, 80*, 810. https://doi.org/10.1007/s12665-021-10117-7

Andersen, T.R.; Poulsen, S.E.; Pagola, M.A.; Medhus, A.B. (2020). Geophysical mapping and 3D geological modelling to support urban planning: a case study from Vejle, Denmark. *Journal of Applied Geophysics, 180,* 104130. https://doi.org/10.1016/j.jappgeo.2020.104130

Arjwech, R.; Sriwangpon, P.; Somchat, K.; Pondthai, P.; Everett, M. (2020). Electrical resistivity tomography (ERT) data for clay mineral mapping. *Data in Brief, 30*, 105494. https://doi.org/10.1016/j.dib.2020.105494

Auken, E.; Christiansen, A.V. (2004). Layered and laterally constrained 2D inversion of resistivity data. *Geophysics, 69*(3), 752-761. https://doi.org/10.1190/1.1759461

Auken, E.; Christiansen, A.V.; Kirkegaard, C.; Fiandaca, G.; Schamper, C.; Behroozmand, A.A.; Binley, A.; Nielsen, E.; Effersø, F.; Christensen, N.B.; Sørensen, K.; Foged, N.; Vignoli, G. (2015). An overview of a highly versatile forward and stable inverse algorithm for airborne, ground-based and borehole electromagnetic and electric data. *Exploration Geophysics, 46*(3), 223-235. https://doi.org/10.1071/EG13097

Azaiez, H.; Gabtni, H.; Chabaane, A.; Sayem, G.; Bédir, M. (2020). Geophysical study of Hammam Sidi Maamar geothermal site in Central Tunisia for sustainable development. *Journal of African Earth Sciences, 170,* 103897. https://doi.org/10.1016/j.jafrearsci.2020.103897

Berezowski, V.; Mallett, X.; Crebert, I.; Seckiner, D.; Ellis, J.; Moffat, I. (2024). A technical protocol for using ground penetrating radar and electrical resistivity tomography in the search for covert graves. *Australian Journal of Forensic Sciences, 56*(5), 534-550. https://doi.org/10.1080/00450618.2023.2252531

Bingham, D.; Legault, J.M. (2018). Geophysics of the Patterson Lake South uranium deposit, northwestern Saskatchewan. *ASEG Extended Abstracts, 2018*(1), 1-6. https://doi.org/10.1071/ASEG2018abW10_3E

Capa-Camacho, X.; Martínez-Pagán, P.; Martínez-Segura, M.; Gabarrón, M.; Faz, Á. (2022). Electrical resistivity tomography (ERT) and geochemical analysis dataset to delimit subsurface affected areas by livestock pig slurry ponds. *Data in Brief, 45,* 108684. https://doi.org/10.1016/j.dib.2022.108684

Chibani, A.; Hebbache, K.; Mellas, M.; Mabrouki, A. (2023). 2D electrical resistivity tomography (ERT) investigation of a landslide: a case study from Ali Mendjeli, Constantine, North-East of Algeria. *NRIAG Journal of Astronomy and Geophysics,*

12(1), 45-57. https://doi.org/10.1080/20909977.2022.2163787

Dastanboo, N.; Li, X.Q.; Gharibdoost, H. (2020). Comparison between electrical resistivity tomography and tunnel seismic prediction 303 methods for detecting the water zone ahead of the tunnel face: a case study. *Open Geosciences, 12*(1), 1094-1104. https://doi.org/10.1515/geo-2020-0193

Doyoro, Y.G.; Chang, P.Y.; Puntu, J.M.; Lin, D.J.; Van Huu, T.; Rahmalia, D.A.; Shie, M.S. (2022). A review of open software resources in python for electrical resistivity modelling. *Geoscience Letters, 9,* 3. https://doi.org/10.1186/s40562-022-00214-1

Finn, C.A.; Bedrosian, P.A.; Holbrook, W.S.; Auken, E.; Bloss, B.R.; Crosbie, J. (2022). Geophysical imaging of the Yellowstone hydrothermal plumbing system. *Nature, 603,* 643-647. https://doi.org/10.1038/s41586-021-04379-1

Genedi, M.; Ghazala, H.; Mohamed, A.; Massoud, U.; Tezkan, B. (2021). Lateral constrained inversion of DC-resistivity data observed at the area north of Tenth of Ramadan City, Egypt for groundwater exploration. *Geosciences, 11*(6), 248. https://doi.org/10.3390/geosciences11060248

Günther, T. (2004). Inversion methods and resolution analysis for the 2D/3D reconstruction of resistivity structures from DC measurements. Ph.D. Thesis, Technische Universität Bergakademie Freiberg, Germany.

Günther, T.; Rücker, C.; Spitzer, K. (2006). Three-dimensional modelling and inversion of DC resistivity data incorporating topography - II. Inversion. *Geophysical Journal International, 166*(2), 506-517. https://doi.org/10.1111/j.1365-246X.2006.03011.x

Hellman, K.; Johansson, S.J.; Olsson, P.O.; Dahlin, T.D. (2016). Resistivity inversion software comparison. *Near Surface Geoscience 2016 - 22nd European Meeting of Environmental and Engineering Geophysics*. Barcelona, Spain. https://doi.org/10.3997/2214-4609.201602016

Idfi, G.; Suryoputro, N.; Laksono, Y.A.; Khomsiati, N.L. (2019). Ground water exploration using geo-electric method for Sumber Cemung pool development. *IOP Conference Series: Materials Science and Engineering, 669*, 012008. https://doi.org/10.1088/1757-899X/669/1/012008

Isaev, I.; Obornev, I.; Obornev, E.; Rodionov, E.; Shimelevich, M.; Dolenko, S. (2022). Multitasking learning in missing data recovery for the integration of geophysical methods in solving an inverse problem of exploration geophysics. *Procedia Computer Science, 213,* 777-784. https://doi.org/10.1016/j.procs.2022.11.134

Jabrane, O.; Azzab, D.E.; Martínez-Pagán, P.; Martínez-Segura, M.A.; Mahjoub, H.; Charroud, M. (2023). Contribution of Python-based BERT software for landslide monitoring using electrical resistivity tomography datasets. a case study in Tghat-Fez (Morocco). *Data in Brief, 46,* 108763. https://doi.org/10.1016/j.dib.2022.108763

Kukemilks, K.; Wagner, J.F. (2021). Detection of preferential water flow by electrical resistivity tomography and self-potential method. *Applied Sciences, 11*(9), 4224. https://doi.org/10.3390/app11094224

Lin, C.; Fiandaca, G.; Auken, E.; Couto, M.A.; Christiansen, A.V. (2019). A discussion of 2D induced polarization effects in airborne electromagnetic and inversion with a robust 1D laterally constrained inversion scheme. *Geophysics, 84*(2), E75-E88. https://doi.org/10.1190/geo2018-0102.1

Loke, M.H.; Barker, R.D. (1996). Rapid least-squares inversion of apparent resistivity pseudosections by a quasi-Newton method. *Geophysical Prospecting, 44*(1), 131-152. https://doi.org/10.1111/j.1365-2478.1996.tb00142.x

Loke, M.H.; Wilkinson, P.B.; Chambers, J.E.; Meldrum, P.I. (2018). Rapid inversion of data from 2D resistivity surveys with electrode displacements. *Geophysical Prospecting, 66*(3), 579-594. https://doi.org/10.1111/1365-2478.12522

Morozov, V.A. (1984). *Methods for Solving Incorrectly Posed Problems.* Springer. https://doi.org/10.1007/978-1-4612-5280-1

Mudler, J.; Hördt, A.; Przyklenk, A.; Fiandaca, G.; Maurya, P.K.; Hauck, C. (2019). Two-dimensional inversion of wideband spectral data from the capacitively coupled resistivity method – first

applications in periglacial environments. *The Cryosphere, 13*(9), 2439-2456. https://doi.org/10.5194/tc-13-2439-2019

Okamoto, K.; Li, B.Q. (2007). Optimal numerical methods for choosing an optimal regularization parameter. *Numerical Heat Transfer, Part B: Fundamentals, 51*(6), 515-533. https://doi.org/10.1080/10407790601128592

Oliveira, L.A.; Braga, M.A.; Prosdocimi, G.; De Souza Cunha, A.; Santana, L.; Da Gama, F. (2023). Improving tailings dam risk management by 3D characterization from resistivity tomography technique: case study in São Paulo – Brazil. *Journal of Applied Geophysics, 210,* 104924. https://doi.org/10.1016/j.jappgeo.2023.104924

Opatola, A.; Obafemi, S.; Bankole, S.I.; Akinwale, R.P.; Alli, S.A. (2022). Geoelectrical resistivity mapping and characterization of bituminous sands at some parts of Eastern Dahomey Basin, SW Nigeria. *Egyptian Journal of Petroleum, 31*(4), 33-38. https://doi.org/10.1016/j.ejpe.2022.10.001

Oraintara, S.; Karl, W.C.; Castanon, D.A.; Nguyen, T.Q. (2000). A method for choosing the regularization parameter in generalized Tikhonov regularized linear inverse problems. *7th IEEE International Conference on Image Processing.* Vancouver. https://doi.org/10.1109/ICIP.2000.900900

Petra, N.; Zhu, H.; Stadler, G.; Hughes, T.J.R.; Ghattas, O. (2012). An inexact Gauss-Newton method for inversion of basal sliding and rheology parameters in a nonlinear Stokes ice sheet model. *Journal of Glaciology, 58*(211), 889-903. https://doi.org/10.3189/2012JoG11J182

Placencia-Gómez, E.; Parviainen, A.; Hokkanen, T.; Loukola-Ruskeeniemi, K. (2010). Integrated geophysical and geochemical study on AMD generation at the Haveri Au–Cu mine tailings, SW Finland. *Environmental Earth Sciences, 61,* 1435-1447. https://doi.org/10.1007/s12665-010-0459-9

Porras, D.; Carrasco, J.; Carrasco, P.; González, P.J. (2022). Imaging extensional fault systems using deep electrical resistivity tomography: a case study of the Baza fault, Betic cordillera, Spain. *Journal of Applied Geophysics, 202,* 104673. https://doi.org/10.1016/j.jappgeo.2022.104673

pyGIMLi. (2023a). 2D ERT modeling and inversion. https://www.pygimli.org/_examples_auto/3_ert/plot_01_ert_2d_mod_inv.html#sphx-glr-examples-auto-3-ert-plot-01-ert-2d-mod-inv-py

pyGIMLi. (2023b). ERT field data with topography. https://www.pygimli.org/_examples_auto/3_ert/plot_02_ert_field_data.html

Quiceno, B.A.; Muñoz, A.M.; Paniagua, J.G.; Bustamante, M.O. (2022). Optimal selection of the regularization parameter for pyGIMLi: geophysical inversion and modeling library. *IEEE ANDESCON.* Barranquilla, Colombia. https://doi.org/10.1109/ANDESCON56260.2022.9989631

Quiceno-Arenas, B.A.; Paniagua-Castrillón, J.G.; Muñoz-García, A.M.; Duque-Gómez, L.F.; Bustamante-Rúa, M.O. (2022). Open-source learning as a skill for geoelectrical data processing: the case of pyGIMLi. *DYNA, 89*(222), 48-53. https://doi.org/10.15446/dyna.v89n222.101826

Redhaounia, B.; Aktarakçi, H.; Ilondo, B.O.; Gabtni, H.; Khomsi, S.; Bédir, M. (2015). Hydro-geophysical interpretation of fractured and karstified limestones reservoirs: a case study from Amdoun region (NW Tunisia) using electrical resistivity tomography, digital elevation model (DEM) and hydro-geochemical approaches. *Journal of African Earth Sciences, 112*(Part A), 328-338. https://doi.org/10.1016/j.jafrearsci.2015.09.020

Reynolds, J.M. (2011). *An introduction to applied and environmental geophysics*. 2dn Edition. Wiley-Blackwell.

Rücker, C. (2011). Advanced electrical resistivity modelling and inversion using unstructured discretization. Ph.D. Thesis, Universität Leipzig, Germany.

Rücker, C.; Günther, T.; Wagner, F.M. (2017). pyGIMLi: an open-source library for modelling and inversion in geophysics. *Computers & Geosciences, 109,* 106-123. https://doi.org/10.1016/j.cageo.2017.07.011

Schenkels, N.; Vanroose, W. (2018). Projected Newton method for a system of Tikhonov-Morozov equations. *arXiv*, 1809.01627. https://doi.org/10.48550/ARXIV.1809.01627

Sirota, D.Y.; Ivanov, V.V. (2018). Diagnostics of the shape and orientation of a rock failure zone based on electrical measurements as an inverse problem

of geophysics. *Russian Geology and Geophysics, 59*(1), 105-109. https://doi.org/10.1016/j.rgg.2018.01.008

Sizikov, V.; Sidorov, D. (2017). Discrete spectrum reconstruction using integral approximation algorithm. *Applied Spectroscopy, 71*(7), 1640-1651. https://doi.org/10.1177/0003702817694181

Sjöberg, Y.; Marklund, P.; Pettersson, R.; Lyon, S.W. (2015). Geophysical mapping of palsa peatland permafrost. *The Cryosphere, 9*(2), 465-478. https://doi.org/10.5194/tc-9-465-2015

Szalai, S.; Szarka, L. (2008). On the classification of surface geoelectric arrays. *Geophysical Prospecting, 56*(2), 159-175. https://doi.org/10.1111/j.1365-2478.2007.00673.x

Szalai, S.; Novák, A.; Szarka, L. (2009). Depth of investigation and vertical resolution of surface geoelectric arrays. *Journal of Environmental and Engineering Geophysics, 14*(1), 15-23. https://doi.org/10.2113/JEEG14.1.15

Tarantola, A. (2005). *Inverse Problem Theory and Methods for Model Parameter Estimation.* Society for Industrial and Applied Mathematics.

Tikhonov, A.N. (1963). On the solution of ill-posed problems and the method of regularization. *Doklady Akademii nauk SSSR, 151*(3), 501-504.

Tikhonov, A.N. (1966). On the stability of the functional optimization problem. *USSR Computational Mathematics and Mathematical Physics, 6*(4), 28-33. https://doi.org/10.1016/0041-5553(66)90003-6

Tikhonov, A.N.; Goncharsky, A.V.; Stepanov, V.V.; Yagola, A.G. (1995). *Numerical Methods for the Solution of Ill-Posed Problems.* Springer Netherlands. https://doi.org/10.1007/978-94-015-8480-7

Von Bülow, R.; Klitzsch, N.; Wellmann, F. (2021). Strategies to overcome near surface disturbances while inverting time-lapse surface ERT data. *Journal of Applied Geophysics, 195,* 104463. https://doi.org/10.1016/j.jappgeo.2021.104463

Wang, Y.; Yagola, A.G.; Yang, C. (2010). *Optimization and Regularization for Computational Inverse Problems and Applications.* Higher Education Press and Springer Verlag.

Willoughby, R.A. (1979). Solutions of Ill-Posed Problems (A. N. Tikhonov and V. Y. Arsenin). *SIAM Review, 21*(2), 266-267. https://doi.org/10.1137/1021044

Wu, C.; He, J.; Zou, X. (2008). A genetic algorithm approach for selecting Tikhonov regularization parameter. *IEEE Congress on Evolutionary Computation (CEC)*, Hong Kong. https://doi.org/10.1109/CEC.2008.4631339

Yonli, H.F.; Koïta, M.; Kanla, I.; Compaoré, A.; Mano, G. (2023). Contribution of electrical resistivity tomography to the anticipation of potential disasters: case of pipe ramming works under road embankments. *Journal of Materials Science and Surface Engineering, 10,* 1091-1096. https://doi.org/10.52687/2348-8956/101

Zamanian, M.; Thorat, Y.A.; Asfaw, N.; Chavda, P.; Shahandashti, M. (2023). Electrical resistivity imaging for identifying critical sulfate concentration zones along highways. *Transportation Research Record: Journal of the Transportation Research Board, 2677*(12), 113-127. https://doi.org/10.1177/03611981231167162

Zeynolabedin, A.; Ghiassi, R.; Norooz, R.; Najib, S.; Fadili, A. (2021). Evaluation of geoelectrical models efficiency for coastal seawater intrusion by applying uncertainty analysis. *Journal of Hydrology, 603*(Part C), 127086. https://doi.org/10.1016/j.jhydrol.2021.127086

Zheng, Z.; Wu, C.; Wang, D. (2019). A novel method for force identification based on filter and FEM. *Journal of Vibration and Control, 25*(19-20), 2656-2666. https://doi.org/10.1177/1077546319866032

Zond Software (2022). ZonRes2D. Manual, Republic of Cyprus.

Received: 20 June 2025
Accepted: 04 February 2026